International Journal of Nanomedicine Dovepress

Open Access Full Text Article ORIGINAL RESEARCH

Controlled Nitric Oxide-Releasing Nanovehicles for Enhanced Infected Wound Healing: A Study on PDA@BNN6 Encapsulated in GelMA Hydrogel

Jing Yang[1,2,*], Donghui Jia[3,*], Jialu Qiao[2,*], Ximing Peng[1], Chuchao Zhou[1], Yanqing Yang[1,*]

[1]Department of Plastic Surgery, Tongren Hospital of Wuhan University (Wuhan Third Hospital), Wuhan, 430060, People's Republic of China; [2]Department of Medicine, Jianghan University, Wuhan, 430056, People's Republic of China; [3]Department of Traumatology, The Third Hospital of Jianghan University, The Huangpi People's Hospital of Wuhan, Wuhan, Hubei, People's Republic of China

*These authors contributed equally to this work

Correspondence: Chuchao Zhou; Yanqing Yang, Email chuchaozhou@sina.com; 202131051063@stu.jhun.edu.cn

Introduction: The photo-activated thermo/gas antimicrobial nanocomposite hydrogel, Gel/PDA@BNN6, is composed of the nitric oxide (NO) carrier N, N'-di-sec-butyl-N, N'-dinitroso-p-phenylenediamine (BNN6), photothermal (PTT) material polydopamine nanoparticles (PDA NPs), and methacrylate gelatin (GelMA). This hydrogel can release NO gas in a stable and controlled manner, generating a localized photothermal effect when exposed to near-infrared laser light. This dual action promotes the healing of full-thickness skin wounds that are infected.

Methods: Gel/PDA@BNN6 was developed, and both in vitro and in vivo experiments were carried out to evaluate its structure, physicochemical properties, antibacterial effects, effectiveness in promoting infected wound healing, and biocompatibility.

Results: Gel/PDA@BNN6 was successfully synthesized, exhibiting a porous three-dimensional lattice structure and excellent mechanical properties. It demonstrated highly efficient photothermal conversion, controllable nitric oxide delivery, strong bactericidal effects, and minimal cytotoxicity in vitro. In vivo, Gel/PDA@BNN6, when used with NIR therapy, showed significant anti-inflammatory effects, promoted collagen deposition, and stimulated vascular neoangiogenesis, which accelerated wound closure. Additionally, it displayed superior biocompatibility.

Discussion: Gel/PDA@BNN6 has shown an explicit curative effect for infected wound healing, suggesting it has a good chance of being an antimicrobial dressing in the future.

Keywords: Nitric oxide, photothermal therapy, infected wound healing, hydrogel, BNN6

Introduction

As a barrier, the skin plays a vital role against dehydration and bacterial invasion and maintains routine metabolic operations. When this barrier is compromised, the body's normal physiological functions may be disrupted by bacterial infection.[1,2] The tissues surrounding wounds in defective skin are susceptible to the formation of necrotic and robust inflammatory responses. In such cases, any growth of proliferation tissue can only occur after the infection has been treated and controlled. The wound takes a long time to heal and often leaves large scars that can hinder the limb's regular functioning.[3–5] Therefore, it is essential to use a dressing that can isolate the wound from its surroundings, moisturize the area, and promote tissue growth while inhibiting pathogens.[6,7]

For the past few years, hydrogels have been widely used in skin wound closure, attributed to their similarity to the cellular microenvironment compared to other dermal wound fillers.[8,9] On the one hand, moisture-rich hydrogels could maintain the wound's hydration level. On the other hand, hydrogels are excellent at sponging wound exudate and are effective in resisting infection.[10] However, its low mechanical strength is a drawback. The emerging GelMA could solidify with ultraviolet (UV) light to enhance mechanical strength and is more suitable for wound strain.[11,12]

Received: 7 September 2024
Accepted: 25 October 2024
Published: 8 November 2024

Additionally, solid GelMA possesses self-healing properties and can endure certain mechanical compression forces.[13] Hu and et al cultured various cell types in GelMA, confirming its excellent biocompatibility and biodegradability.[14] Whereas GelMA has minimal antimicrobial capacity, introducing antimicrobial materials is necessary.

Studies indicate that NO is a potential antimicrobial agent for multiple bacteria, both gram-positive and gram-negative, due to its ability to damage bacterial membranes and DNA.[15–17] Meanwhile, as an essential regulator, NO positively impacts all phases of the injury repair process.[18] In the inflammatory response phase, NO as an inflammatory mediator regulates the generation and delivery of pro-inflammatory cytokines, such as IL-1, IL-6, and TNF-α.[19,20] During tissue reconstruction, NO stimulates myofibroblast proliferation and migration, and promotes collagen neogenesis and deposition, thus enhancing vascularization.[18] Recently, many studies have shown that mice missing endothelial NO synthase (eNOS) or inducible NO synthase (iNOS) exhibited decreased neovascularization and delayed wound healing.[21,22] Whether NO is a pro-inflammatory cytokine or an anti-inflammatory cytokine is still controversial. Some scholars believe that NO has some pro-inflammatory effects.[23] However recent studies have shown that NO is more inclined to be an anti-inflammatory cytokine.[24,25] Besides, NO dilates blood vessels to deliver nutrients to damaged tissue and expedites metabolism. Although NO has unique properties in wound repair, its explosive release limits its popularization and application. It is essential to build stable NO-delivery platforms for precise and controlled release of NO. In previous studies, researchers have utilized various exogenous triggers, including light irradiation, the potential of hydrogen, enzyme catalysis, and thermocatalytic, to investigate the NO release from small-molecule NO donors.[26,27] BNN6, a low-toxicity substance, is an accessible NO donor that releases NO upon UV exposure. It has recently been utilized to treat infected wounds.[28,29]

To meet the requirement of controlled-release NO, we attempted to combine an NO donor with NIR laser-mediated PTT. When exposed to NIR light, photothermal agents (PTAs) produce heat energy that damages bacterial cell membranes and denatures proteins. Using physical heat to kill bacteria has less potential to induce multidrug-resistant microbes.[30] Among the various PTAs, PDA NPs are a significant nanocarrier due to their superior photostability, controllability, and promising biocompatibility.[31] Furthermore, the potential of PDA NPs for NIR-stimulated production NO deriving from BNN6 is suggested by its powerful photoconductivity, light-gathering, electron-transfer capabilities, and conjugated π structure.[32] However, the single PDA NPs are too aggregated to improve photothermal conversion efficiency, and normal tissues have limited capacity to withstand high temperatures. Combining the PDA NPs and BNN6 through π-π stacking interactions is hopeful for resolving this issue and effective sterilization.

Herein, we designed to develop BNN6-functionalized PDA nanocomposites dispersed in GelMA to promote infectious wound healing (Scheme 1). We loaded BNN6 onto the surface of PDA NPs, forming PDA@BNN6 nanocomposites, which were then encapsulated in GelMA. This way, we got Gel/PDA@BNN6 with photoactivated thermal/gas antibacterial activity, releasing NO gas and producing local hyperthermia with the 808 nm laser. The composite hydrogel synthesis was clarified using a battery of spectral analysis and imaging processes. The multi-functional hydrogel exhibited superior antibacterial activity compared with other groups due to the synergistic effect of the gas-photothermal strategy. The hydrogel has been demonstrated to be non-toxic in both cytocompatibility tests in vitro and rat models. Especially during the treatment of infected wounds, the measure shows positive effects through thermotherapy, anti-inflammatory effects, and promoting collagen deposition. Overall, this study presents a promising dual-modal antibacterial therapeutic strategy that uses photothermal and gas to target infected wounds accurately.

Materials and Methods

Materials

Dopamine hydrochloride (DA • HCl, 97.5%), N, N′-bis-sec-butylamino-p-phenylenediamine (BPA, 95%), Dimethyl sulfoxide (DMSO), Sodium nitrite ($NaNO_2$), hydrochloric acid (HCl), anhydrous ethanol(C_2H_5OH), oxyammonia (NH_4OH, 28–30%) and phosphate-buffered saline (PBS, PH=7.4) were purchased from Sigma-Aldrich (Shanghai, China). GelMA was obtained from Engineering for Life (Suzhou, China). *S. aureus* (CMCC 26003) and *E. coli* (CMCC 44102) were purchased from the Bioresource Collection Center (Shanghai, China). Calcein-AM and propidium iodide (PI) were obtained from Solarbio Science & Technology Co., Ltd. (Beijing, China). The cell counting assay kit-8 (CCK-8) was bought from Servicebio (Wuhan, China).

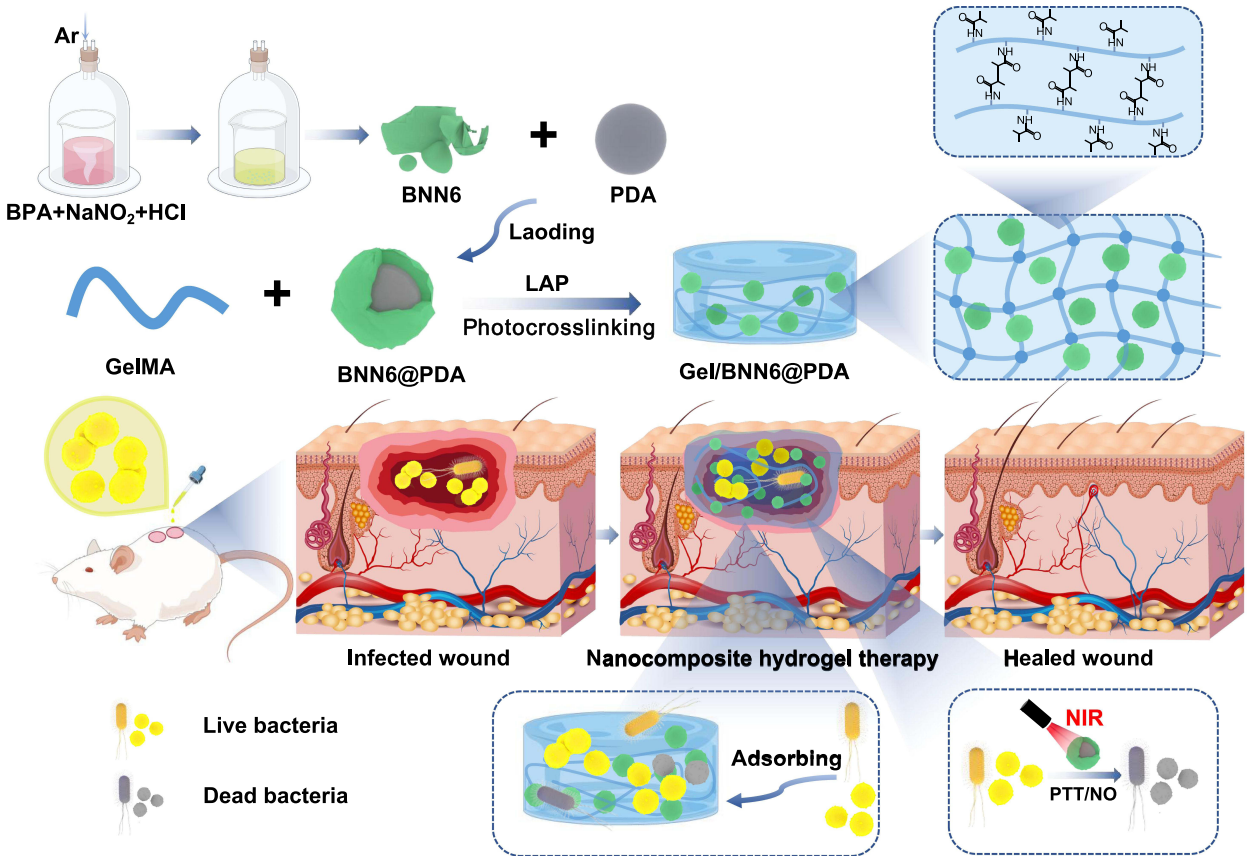

Scheme 1 Schematic of Gel/PDA@BNN6 synthesis and its use in treating infected wounds.

Synthesis of BNN6

BNN6 was synthesized in the following procedure. 1.17mL of BPA (5mM) was dissolved in 9 mL of Ethyl alcohol. Next, 10 mL of $NaNO_2$ (6M) was gradually dropped into the solution surrounded by argon and agitated continuously for 30 minutes. After adding 10 mL of HCl (6M), the solution turned orange, producing a beige sediment. A 4-hour stirring process was followed. The solution was centrifuged and washed several times, and the lyophilized product was stored at −20 °C.

Synthesis of PDA NPs

This method has been previously reported.[33] First, 90 mL of deionized (DI) water was mixed with 40 mL of anhydrous ethanol at room temperature and stirred well. Then, 5 mL of oxyammonia was added to the mixture and stirred for 30 minutes at room temperature to obtain a uniform solution. Afterward, 500 mg of dopamine hydrochloride was dissolved in 10 mL DI water. The resulting solution was added to the mixed solution and kept in darkness for 24 hours to allow for a spontaneous reaction to occur. The precipitate was collected by centrifugation at 12,000 rpm for 30 minutes, then washed and centrifuged with DI water five times until the supernatant was clarified. Finally, the PDA NP precipitate was lyophilized for further use.

Synthesis of PDA@BNN6 Nanoparticles and Loading Capacity

Various amounts of BNN6 (0.4mg, 0.8mg, 1.2mg, 1.6mg, 2mg) were dissolved in 4 mL of ethanol (33%). Subsequently, 3mg of PDA NPs was dissolved in a 6 mL DMSO solution with constant stirring. The BNN6 solution was gradually added to the PDA NPs solution while stirring continuously for 12 hours in the dark. The solution was then left undisturbed for 3 hours to allow for complete self-assembly. The precipitate was collected through centrifugation at 12,000 rpm, washed thrice with deionized water, and the PDA@BNN6 composite

particles were obtained by freeze-drying them and storing them at −20°C. The Loading efficiency was determined by collecting the upper layer of waste liquid and measuring the remaining BNN6 using UV-visible spectroscopy.

$$\text{Loading efficiency } (\%) = \frac{C_0 \times V_0 - C_e \times V_e}{m} \times 100\%$$

C_0 (μg mL^{-1}) and C_e (μg mL^{-1}) represent the initial and final concentrations of the BNN6 solution, respectively. V_0 (mL) and V_e represent the initial and final volumes of the liquid, and m (mg) denotes the mass of the PDA NPs.

Synthesis of the Hydrogels

GelMA (200 mg) was solubilized in 4 mL of PBS by magnetic agitation at 37°C (5% wv−[1]) to obtain the hydrogel. Next, a certain proportion of BNN6, PDA NPs, or PDA@BNN6 nanoparticles were added separately and stirred for 5 min. Then, 20 mg of phenyl-2,4,6-trimethylbenzoyl phosphonate lithium (0.5% wv−[1]) was added, and the mixture was crosslinked quickly by irradiating it with a 405 nm blue light for 45 seconds.

Characterization of These Materials

The surface morphologies were analyzed using scanning electron microscopy (SEM; UK ZEISS, Sigma, England). The molecular structure of the BNN6 was confirmed using Hydrogen Nuclear Magnetic Resonance.[1] H NMR; Bruker, 400 MHz, Germany The particle size distribution was measured on a Zetasizer Nano ZS (Malvern, UK). Fourier transform infrared spectrometry (FT-IR) data were obtained using an infrared microscope (VERTEX 70, German). UV-visible (UV-vis) spectra were measured with a UV spectrophotometer (Shimadzu UV-2600, Japan). Using an X-ray powder diffractometer (XRD, Ultima IV, Japan), the X-ray diffraction patterns with angles from 5 to 80° were drawn. Raman spectrometers were used to record the structural changes (BWS465-785S, BWTEK, American). The temperature of the samples was monitored using an infrared thermal camera (HM-5202ZC2, China).

Rheological Characteristics of GelMA and Gel/PDA@BNN6

Rheological characteristics of GelMA and Gel/PDA@BNN6 were tested using a rotational rheometer (Haake Mars III, Germany) at 25°C. Storage modulus(G') and loss modulus(G") were measured during the photocurable process of both hydrogels to analyze their mechanical strength changes. To assess the hydrogels' capacity to recover and withstand fatigue, they were squeezed at a low strain of 1% for one minute, followed by a high strain of 400% for another minute at a frequency of 1 hz, and a cycling experiment. A dynamic frequency sweep was performed with a steady strain of 1% using the 0.1–10 hz range. The viscosity response of the hydrogels was monitored for 1 minute at a low shear rate of 0.1 s^{-1}.

Photothermal Effect in vitro

Testing the photothermal efficiency of nanoparticles: 0.5 mL each of PBS solution, PDA NPs (240 μg mL^{-1}), and PDA@BNN6 (400 μg mL^{-1}, with equivalent PDA concentration) were exposed to 808 nm NIR (laser density 1.5 W cm^{-2} 5 min), and temperature changes were recorded every 30s using an infrared camera. We also test the hydrogels for photothermal properties. 0.5 mL each of GelMA, Gel/PDA (240 μg mL^{-1}), and Gel/PDA@BNN6 (400 μg mL^{-1}, with equivalent PDA concentration) were exposed to 808 nm NIR (1.5 W cm^{-2} 5 min) while the temperature change was recorded. In addition, 808 nm NIR of different density powers (0, 0.5, 1, and 1.5 W cm^{-2}) were used to irradiate the Gel/PDA@BNN6 to understand the photothermal influences on this hydrogel. Finally, the photothermal stability of Gel/PDA@BNN6 with NIR was evaluated. The hydrogels were exposed to 808 nm NIR (1.5 W cm^{-2}) for 9 minutes and then cooled down for 9 minutes to cool to temperature under normal conditions. The time-temperature curve was plotted after repeating the cyclic heating and cooling process four cyclic.

NO Release Effect in vitro

A commercial Griess assay kit (Beyotime Biotechnology, China) was used to detect NO release. The concentration of $NaNO_2$ will be diluted to (20, 40, 60, 80, and 100 μM) using PBS solution and treated with the Griess reagent. The post-treatment liquid's absorbance at 540 nm will be measured to plot the standard nitrogen concentration corresponding absorbance curve.

PBS solution, BNN6(160 μg mL^{-1}), and PDA@BNN6 (400 μg mL^{-1}, with equivalent BNN6 concentration) were exposed to 808 nm NIR (1.5 W cm^{-2} min). Every 6 minutes, 50 μL of liquid was taken and treated with the Griess reagent. The absorbance was measured to calculate the amount of NO released. The Gel/PDA@BNN6 (1000 μg mL^{-1}) was studied for its NO release properties under continuous or intermittent NIR irradiation using the same method.

Antibacterial Activity Assay in vitro

S. aureus and *E. coli* are used to assess the antibacterial activity of the hydrogels in vitro. 200 μL of each of the hydrogels was singly added to the Eppendorf tube and sterilized, and 100 μL of bacterial suspension (1×10^8CFU mL^{-1}) was added to the surface of the hydrogel and co-incubated overnight at 37°C. These hydrogels were exposed with or without NIR laser (808 nm, 1.5 W cm^{-2}, 5 minutes). We conducted the plate counting assay and the bacterial live/dead staining assay for the hydrogel-treated bacterial samples, respectively. The untreated bacterial suspension was considered the control group.

The hydrogel-treated bacterial solution was collected and diluted to 1000 fold, and 100 μL of the suspension was taken to spread evenly on fresh broth agar plates. After incubating for 24 hours, bacterial colonies were enumerated.

In addition, we collected hydrogel-treated bacteria and quantified them to 200 μL. After staining the bacteria with the SYTO 9/PI Live/Dead Bacterial Double Stain Kit, fluorescence images were captured by fluorescent microscopy.

Cell Culture and Cytotoxicity Assay

The cytotoxicity of the hydrogels against Human immortalized keratinocytes (HaCaT cells) was evaluated in vitro. HaCaT cells were provided by the Cell Bank of the Chinese Academy of Sciences (Shanghai, China). Dulbecco's modified Eagle's medium (DMEM) and fetal bovine serum (FBS) were supplied by Hyclone (Logan, USA). HaCaT cells were maintained in DMEM supplemented with 10% FBS at 37°C and 5% CO_2. To obtain the leach liquor, 2 mL of the hydrogels were immersed in 10 mL of culture medium for 24 hours (37°C, 5% CO_2). The untreated culture medium was considered to control. The HaCaT cells were incubated within the leachate for 4, 24, and 48 hours.

Cultured cells were treated with a calcein-AM/PI live/dead cell double staining kit and photographed using fluorescence microscopy to obtain the relative calcein-AM fluorescence ratio, which is used to assess cell proliferation trends.

At various times during the incubation, the old medium was replaced with 200 μL of CCK-8 solution (20 μL CCK-8, 180 μL culture medium). The cells were then incubated in the dark for 4 hours, and the optical density (OD) value at 450 nm was measured. Thus, the effect of various hydrogel treatments on cell viability was analyzed.

$$\text{Cell viability}(\%) = \frac{A_x - A}{A_0 - A} \times 100\%$$

A: The OD value at 450 nm of CCK-8 solution.

A_x: The OD value at 450 nm of cells incubated with CCK-8 solution after incubation with the DMEM leachate of the different materials.

A_0: The OD value at 450 nm of cells incubated with CCK-8 solution after incubation with the untreated DMEM.

Degradation Characteristics

During degradation testing, hydrogels were placed in 10 mL of PBS (pH 7.4, 37°C) and shaken at 150 rpm. Photographs were taken, and weight was recorded every two days to document the degradation process.

Wound Healing Experiment in vivo

All animal experiments were approved by the Animal Ethics Committee at Tongren Hospital, Wuhan University. The study complied with the National Research Council's Guide for the Care and Use of Laboratory Animals. Male Sprague-Dawley rats weighing 250–300g were anesthetized, and a circular 8 mm diameter wound was made after shaving the dorsal fur. Each wound was inoculated with 10μL of *S. aureus* suspension (1×10^8 CFU mL^{-1}) to create models of infected skin defects. The rats were randomly distributed to different sections (Control, GelMA, Gel/PDA@BNN6, Gel/BNN6+NIR, Gel/PDA+NIR, and Gel/PDA@BNN6+NIR) to be handled separately. 808 nm NIR (1.0W cm^{-2}) was

irradiated for 3 minutes to record the photothermal changes in the hydrogels. The rats' wound healing process was monitored by photographing the infected wounds on various days.

Histological and Analysis

On the 12th day of the wound healing experiment, each group's skin tissue surrounding the wound site was collected and fixed in 4% formaldehyde for 24 h. Then, they were embedded in paraffin and sectioned to 5μm thick for hematoxylin-eosin (H&E) staining, Masson's staining, immunohistochemistry (IL-6 and CD163) staining, and double immunofluorescence (CD31 and α-SMA) staining (Servicebio, 1359857).

Biocompatibility in vivo

To evaluate the biocompatibility of hydrogel dressings, we collected rat blood for liver and kidney function tests at 12 days postoperatively. At the same time, the rats' organs (heart, liver, spleen, kidney, and lung) were collected and processed for tissue examination by staining with H&E.

Statistical Analysis

The quantitative data obtained from all results were expressed as mean ± standard deviation ($n \geq 3$). For statistical analysis, GraphPad Prism 9.0 was used. Student's *t*-test was performed to compare the means of two groups, whereas analysis of variance (ANOVA) tests were used to compare multiple groups.

Results and Discussions

Characterization of BNN6, PDA and PDA@BNN6 Nanoparticles

BNN6 has been reported to release NO through UV treatment. We synthesized BNN6 and demonstrated that when it was exposed to UV light (405 nm), the DMSO solution of BNN6 changed from light yellow to red. This change indicated that NO and BHA were formed through photochemical reactions (Figure S1).[34] Based on the ^{1}H NMR results of Figure S2, BNN6 was confirmed to have been successfully synthesized again. PDA NPs act as a photothermal agent capable of releasing heat. Combining the two materials, BNN6 and PDA NPs, promotes NO release from BNN6 while exerting a dual-action antimicrobial effect. We obtained scanning electron microscope (SEM) images of the NO donor BNN6, photothermal agents PDA NPs, and PDA@BNN6 nanocomposites, respectively. The results indicated that PDA NPs and PDA@BNN6 nanocomposites are regular spherical nanoparticles, while BNN6 has an irregular shape (Figure 1A). The particles size distribution result, consistent with electron microscopy, displayed that the diameter of PDA NPs was about 170–190 nm. After loading with BNN6, the diameter distribution of the PDA@BNN6 nanocomposites was in the range of 295–531nm (Figure 1B). FT-IR spectroscopy confirmed successfully loaded BNN6 on PDA NPs. As shown in Figure 1C, the presence of PDA NPs is reflected in -OH stretching vibrations of the broad peaks at 3200 cm^{-1} and C=C stretching vibrations at 1610 cm^{-1}.[35] Typical peaks in the spectrum of BNN6 were at 1377 cm^{-1}, which are caused by the shear vibration of N-N=O.[36] At 1120 cm^{-1}, a superposition stretching vibration of C-N on the benzene ring of BNN6 and C-O of PDA NPs forms the absorption peak. Moreover, the peaks observed at 1450 and 1290 cm^{-1} may be attributed to the stretching vibration of the C-N bond. The 2974, 2935, and 2878 cm^{-1} peaks suggested the presence of the sec-butyl group in BNN6, which partially overlaps with the broad peak characteristic of PDA NPs.

In addition, the near-infrared absorption spectra of the aqueous solution of PDA@BNN6 did not change after 7 days of storage at room temperature, indicating that the PDA@BNN6 nanoparticles had good stability. Given the typical absorption peak of BNN6 at around 260 nm in the UV-vis spectrum, we plotted the Concentration-absorbance standard curve of BNN6 concentration by quantitative analysis (Figure 1D and Figure S3). Following this, we found that the BNN6 loading efficiency in PDA@BNN6 nanocomposites followed a concentration-dependent equation shown in Figure 1E. For cost savings, the concentration of BNN6 was set at 200 μg mL^{-1}, corresponding to a BNN6 loading percentage of 40.25%.

In the photothermal effect tests, PDA NPs increased the temperature by 35.3 °C after being exposed to an 808 nm NIR laser for 5 minutes. The same dose of PDA nanoparticle pellets loaded with BNN6 increased the temperature by 38.2 °C (Figure 1F). We observed that pure PDA NPs in PBS solution tend to aggregate spontaneously, whereas

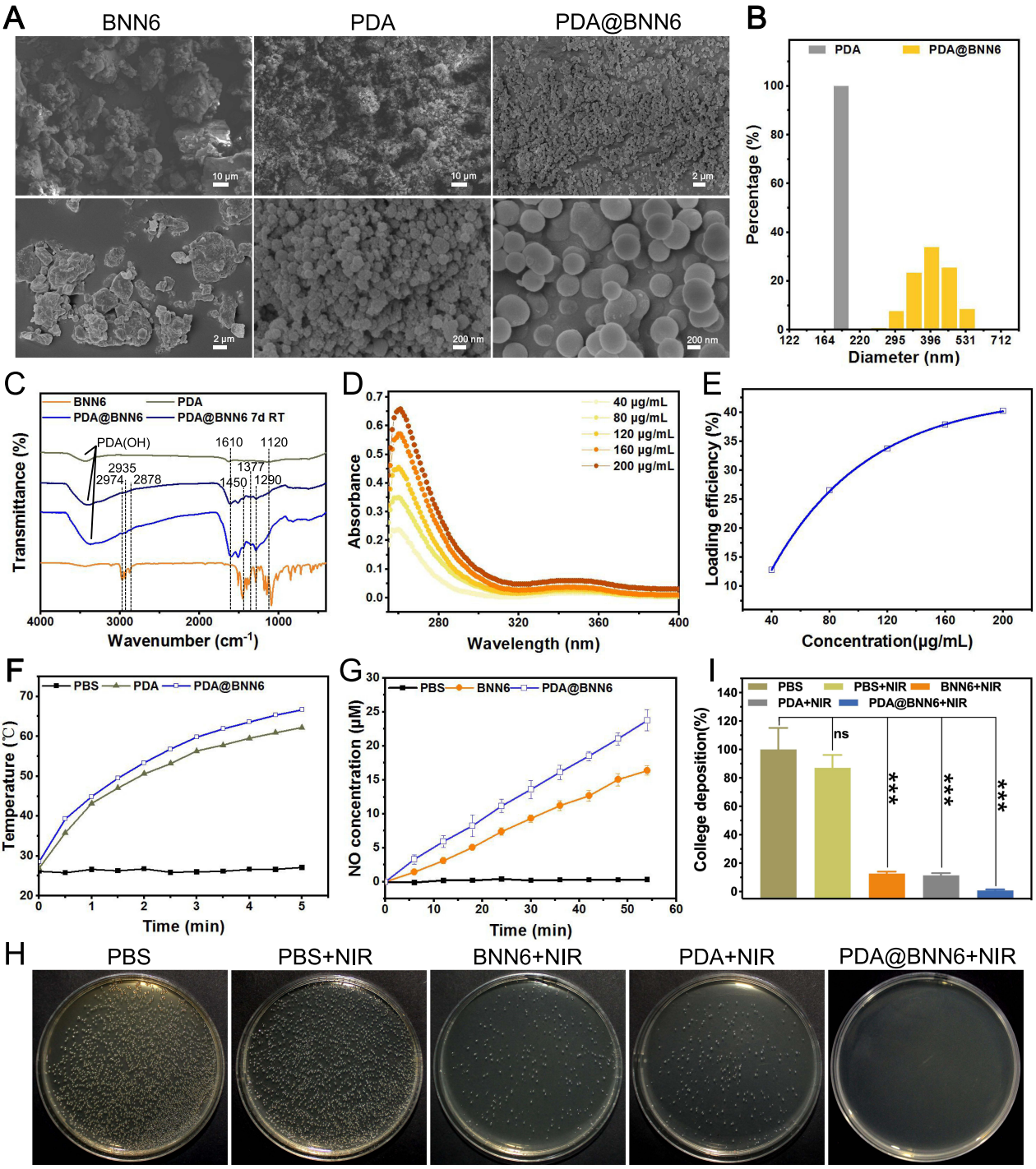

Figure 1 Characterization of PDA@BNN6 nanoparticles. (**A**) SEM images. (**B**) Particle size distribution. (**C**) FT-IR spectra. (**D**) UV-Vis spectra of BNN6; (**E**) BNN6 loading efficiencies for PDA at various BNN6 concentrations. (**F**) Temperature change curves and (**G**) NO concentration of PBS, BNN6, PDA, and PDA@BNN6 under NIR laser irradiation (1.5 W cm^{-2}). (**H-I**) Pictures of agar plates of treated *S. aureus* colonies and corresponding statistics. (n=3, ns means not significant, and ***P < 0.001).

PDA@BNN6 particles are deposited at a slower rate. The higher dispersion of PDA NPs after loading BNN6 might explain the better photothermal effect. For testing NO release behavior, Griess's classic assay technique was used. A standard curve for NO was established, as shown in Figure S4. After 54 minutes of irradiation with near-infrared light, the BNN6 solution released 16.4 μM of nitric oxide, while the PDA@BNN6 solution released 23.79 μM (Figure 1G). The NIR light and the Photothermal agent-mediated Photothermal conversion procedure improved the efficiency of NO

release from BNN6. Whereafter, we used *S. aureus* to test the antimicrobial effect of PDA@BNN6 nanoparticles. As shown in (Figure 1H and I), BNN6+NIR, PDA+NIR, and PDA@BNN6 +NIR exhibited clear sterilisation capabilities. Taken together, PDA@BNN6 composite nanoparticles have been successfully synthesized, demonstrating improved homogeneity, photothermal conversion performance, and more efficient NO release.

Characterization of GelMA, Gel/BNN6, Gel/PDA and Gel/PDA@BNN6

To further obtain functionalized hydrogels, we incorporated BNN6, PDA NPs, and BNN6@PDA nanocomposites into GelMA, respectively. As depicted in Figure 2A, each hydrogel was a cylinder with a diameter of 8 mm at the base and a height of 2 mm. The unloaded GelMA was colorless, while the Gel/BNN6 was faint yellow, the Gel/PDA was black,

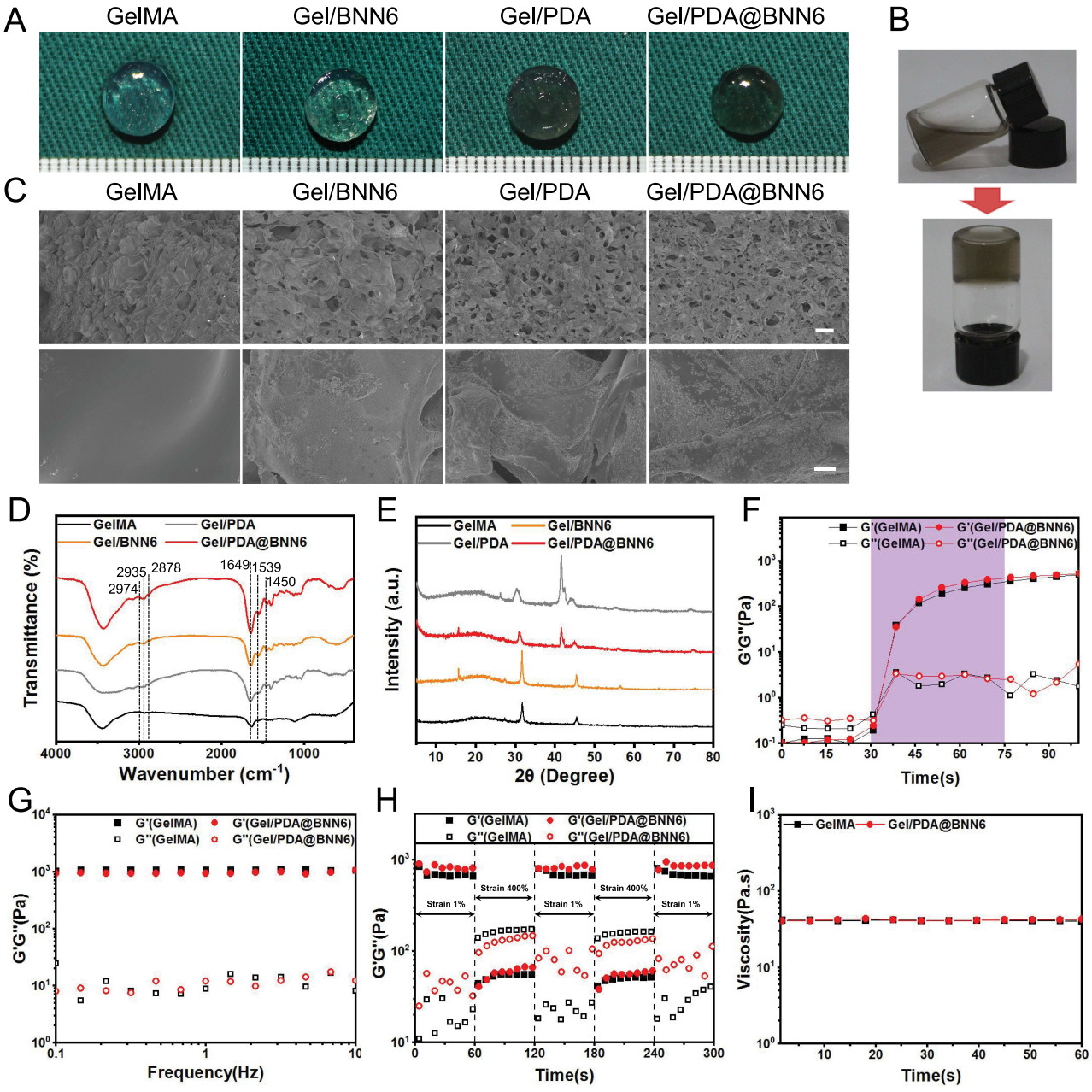

Figure 2 Characterization of hydrogels. (**A**) Optical images. (**B**) Gel/PDA@BNN6 solidify process. (**C**) SEM images at low (Mag = 100×, scale bar: 100 μm), and high (Mag = 2000×, scale bar: 5 μm) magnifications. (**D**) FT-IR spectra. (**E**) XRD patterns. (**F-I**) Rheological performance: Photocurable process sweep, frequency sweep, dynamic step strain sweep, and viscosity measurements for GelMA and Gel/PDA@BNN6, respectively.

and the Gel/PDA@BNN6 was gray-black. After blue light irradiation 45s, the flowing liquid solidifies to form a hydrogel solid with specific mechanical properties (Figure 2B). When observed under scanning electron microscopy (Figure 2C), all hydrogels had a porous three-dimensional lattice structure that helped facilitate material exchange. The honeycomb-like interconnected porous structure can facilitate the transport of substances, promote cell adhesion and proliferation,[10] and provide a pathway for the permeation of nitric oxide. GelMA had a smooth surface, while Gel/BNN6, Gel/PDA, and Gel/PDA@BNN6 had rough particles on their surfaces, indicating the successful incorporation of antimicrobial materials into the hydrogels. Infrared spectrums revealed vibration peaks at 1539 cm^{-1} and 1649 cm^{-1}(Figure 2D), resulting from the amide in GelMA and the stretching vibration peak of C = O, which were also evident in all hydrogels.[37] GelMA and PDA NPs display wide OH stretching peaks at approximately 3300 cm^{-1} and 3200 cm^{-1} in several, which remain unchanged in the Gel/PDA spectra. This result indicates that blending GelMA with the above materials did not alter their chemical properties. The XRD pattern of GelMA showed a broad peak at $2\theta = 23.5°$, which was also present in the other three hydrogels (Figure 2E). That proved that the crystalline structure of GelMA was untouched during the compounding with these particles.[38] In Raman spectroscopy analysis, GelMA showed the amide A peak corresponding to the N-H and O-H stretching without any obvious blue-shift or red-shift for all four hydrogels,[39,40] indicating no damage to the molecular structure of the hydrogels (Figure S5).

Rheological analysis is utilized to evaluate the mechanical properties of hydrogels in order to determine their effectiveness as wound dressings. During the photocurable process, GelMA and Gel/PDA@BNN6 exhibited a lower storage modulus (G') than loss modulus (G") before blue light radiation. This is the moment both hydrogels' viscosity dominates, indicating them in a liquid state. After 45 seconds of irradiation, the G' of Gel/PDA@BNN6 became much higher than G", turning into a gel state where elastic behavior dominates. However, it took longer for GelMA to reach the same G' (Figure 2F). During the dynamic frequency sweep test, the frequency was in the range of 0.1 to 10 hz. The results indicated that both GelMA and Gel/PDA@BNN6 hydrogels maintained stable G' and G" values throughout the test. The G' was consistently higher than the G" (Figure 2G), suggesting that both hydrogels had stable elastic behavior after cross-linking. In the strain sweep experiment, the breakpoint for Gel/PDA@BNN6 was around 23.5% (Figure S6). During the study, GelMA and Gel/PDA@BNN6 were tested for their recoverability by subjecting them to alternating low and high strains (Figure 2H). Results showed that at high strains, both hydrogels had a higher G" than G', which means their gel-like behavior changed to a sol-gel-like behavior.[41] Moreover, the behavior quickly returned to normal when the strains were reduced. After two cycles, there was no wastage of G' in either hydrogel, indicating that both hydrogels had superior fatigue resistance and self-repairing ability.[42] In addition, we discovered that the viscosity measurements of GelMA and Gel/PDA@BNN6 were consistent (Figure 2I). In other words, GelMA and Gel/PDA@BNN6 showed consistency in the photocurable process, strain testing, and viscosity analysis. That indicated that the physical blend of PDA@BNN6 Nanoparticles had no impact on the rheological properties of GelMA. The above results indicate that the composite PDA@BNN6 nanoparticles have been effectively incorporated into GelMA. The modified solid hydrogel exhibits adequate viscosity, elasticity, and stable compressive capacity.

Photothermal and NO Release Performance of Gel/PDA@BNN6

Next, we conducted photothermal monitoring to test whether Gel/PDA@BNN6 still has good photothermal performance. It is observed that GelMA's temperature change was almost negligible after being exposed to NIR for 5 minutes. In contrast, the temperature of Gel/PDA rose from 23.3 to 63.1 °C, and the temperature of Gel/PDA@BNN6 rose from 23.7 to 66.1 °C in Figure 3A and B. As exhibited in Figure 3C and D, the temperature of Gel/PDA@BNN6 was higher with the power of the NIR, which meant that the temperature of the Gel/PDA@BNN6 was tunable. After repeated heating for four cycles, the Gel/PDA@BNN6 was still able to maintain high photothermal efficiency, indicating profitable photothermal stability (Figure 3E).

During continuous exposure to 808 nm laser irradiation, the Gel/PDA@BNN6 released 58.87 μM of nitric oxide in 54 minutes. In intermittent NIR laser irradiation, nitric oxide production rapidly increased when Gel/PDA@BNN6 was exposed to NIR irradiation, and it decreased almost wholly when the NIR was turned off. Once exposed again, the gas was released rapidly (Figure 3F). The results of these three cycles indicated that the successful synthesis of Gel/PDA@BNN6 achieved a controlled release of nitric oxide. In the above tests, Gel/PDA@BNN6 showed satisfactory photothermal efficiency and stability, power-adjustable temperature, and on/off release of NO gas under near-infrared light.

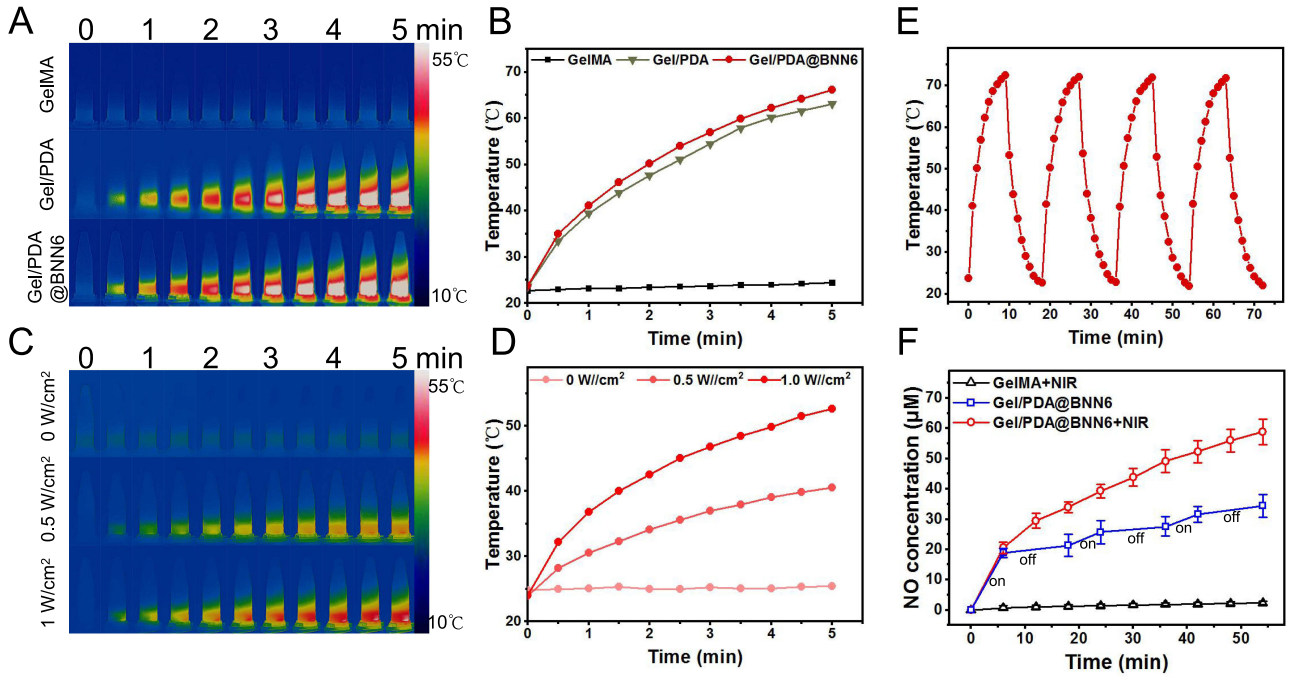

Figure 3 Photothermal effect and NO release properties in vitro. (**A**) Thermal images of hydrogels and (**B**) corresponding temperature variation. (**C**) Photothermal images of Gel/PDA@BNN6 exposed to different levels of NIR irradiation and (**D**) the corresponding temperature variation curve. (**E**) The irradiation cycle experiment of Gel/PDA@BNN6. (**F**) NO concentration of hydrogels exposed to continuous or intermittent NIR irradiation (808 nm, 1.5 W cm-2, n=3).

Antibacterial Activity in vitro

As an advanced composite material, Gel/PDA@BNN6 has a potent antibacterial ability against a broad spectrum of bacteria. We selected *S. aureus* and *E. coli* as model organisms to assess the antimicrobial properties of the samples. All hydrogels respectively treated the bacteria with or without NIR exposure. As depicted in Figure 4A–D, the colony number of the Control and GelMA groups had almost no effect with or without NIR irradiation, implying that NIR alone did not prevent colony propagation. After NIR irradiation, the bacterial viability rate was significantly lower in the Gel/PDA group, with 4.6% for *S. aureus* and 1.4% for *E. coli*. This result demonstrates that PDA NPs could raise the temperature of GelMA, leading to sterilization. The bacterial viability rate in the Gel/PDA@BNN6 with NIR irradiation group was 0.3% for *S. aureus* and 0.1% for *E. coli*, which was lower than that in the Gel/PDA with NIR group, indicating that the hydrogel's antimicrobial ability was more optimized after loading BNN6. In addition, non-NIR irradiated groups Control and Gel/BNN6 showed a significant difference in bacterial survival, suggesting that NO release also significantly affected bacterial survival, which was more reduced in NIR irradiation. This evidence suggested that the Gel/PDA@BNN6 with NIR irradiation has excellent sterilization properties because PDA NPs' superior photothermal conversion efficiency cooperated with the NO pro-release mechanism.

To explore the anti-bacterial mechanism of composite nanoparticle hydrogel further, we used the SYTO 9/PI Live/Dead Bacterial Double Stain Kit obtained from Maokang Biotechnology Co., Ltd (Shanghai, China). The SYTO 9 stains the nucleic acid of live bacteria by penetrating the membrane displayed green fluorescence. The PI stains the dead bacteria only with a ruptured membrane, which shows red fluorescence.[43] As shown in Figure 4E–H, in the Control and GelMA groups, most of the two types of bacteria survived. On the contrary, most bacteria died after Gel/BNN6, Gel/PDA, or Gel/PDA@BNN6 treatments, especially after exposure to NIR irradiation. The Gel/PDA@BNN6 with NIR group exhibited the highest inhibitory efficiency, resulting in bacterial activities of 0.74% for *S. aureus* and 0.34% for *E. coli*. The live/dead cell assay trend was consistent with the plate count results. Photothermal action synergizes with NO to cause severe disruption to the bacterial cell membrane, resulting in sterilization. In summary, Gel/PDA@BNN6 combined with NIR irradiation demonstrated excellent antimicrobial effects in this part of the assay.

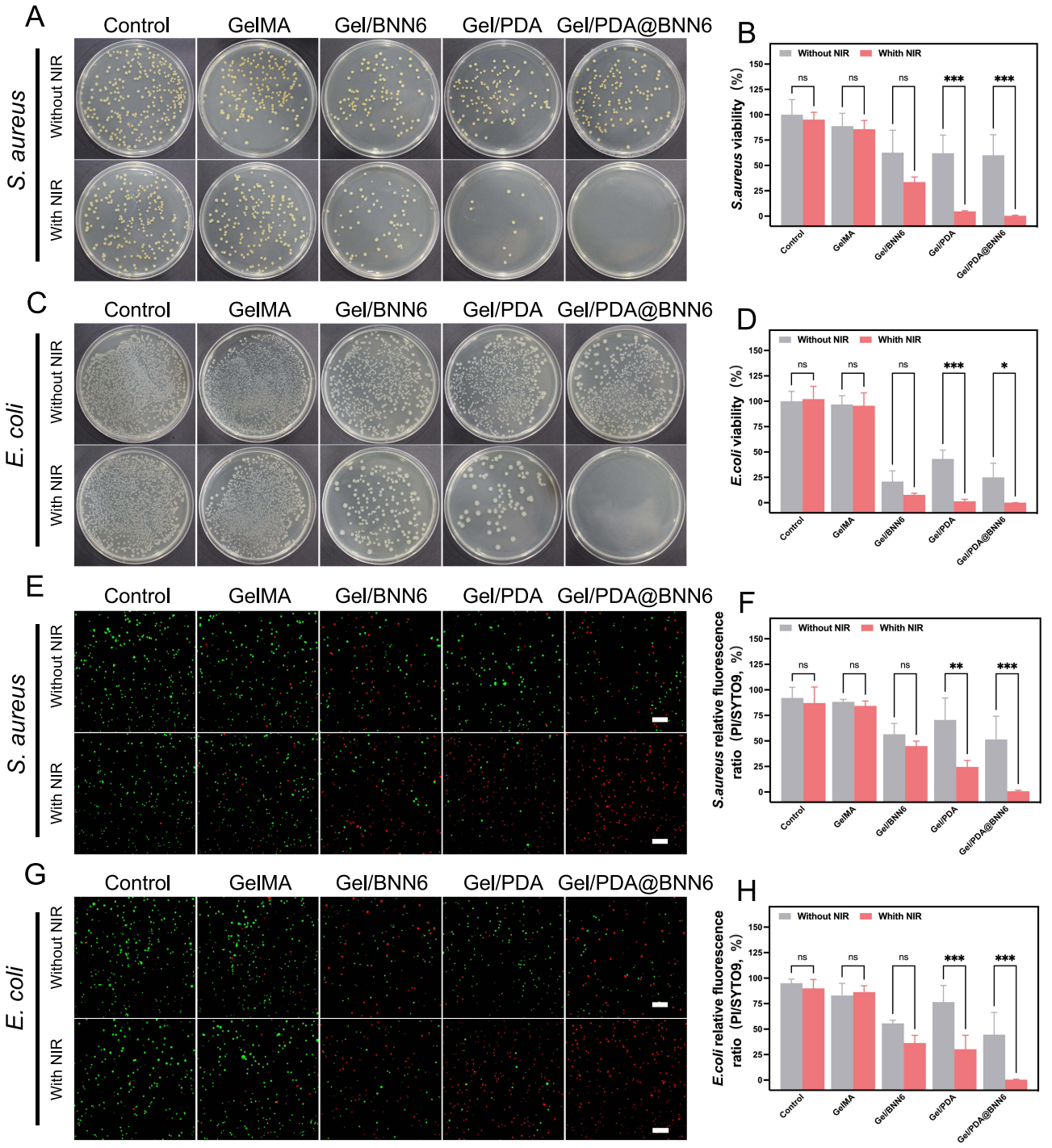

Figure 4 In vitro antibacterial activity against *S. aureus* and *E. coli*. (**A**) and (**C**) The treated colony growth representative images. (**B**) and (**D**) Statistical data of colony counts. (**E**) and (**G**) Confocal fluorescence (scale bars: 20 μm). (**F**) and (**H**) Relative fluorescence ratios of different samples. (n = 3, ns means not significant, *P < 0.05, **P < 0.01, and ***P < 0.001).

Cytotoxicity Assay and Degradation Characteristics in vitro

Favorable cytocompatibility is an inevitable requirement for drugs. The Calcein-AM/PI double stain kit was used to monitor cell replication and assess biocompatibility. Green fluorescence was observed within living cells using Calcein-AM, while red fluorescence was observed within dead cells using PI. After 4, 24, and 48 hours of co-culture, the number of living HaCaT cells increased progressively in all groups, and almost no dead cells were found (Figure 5A and B),

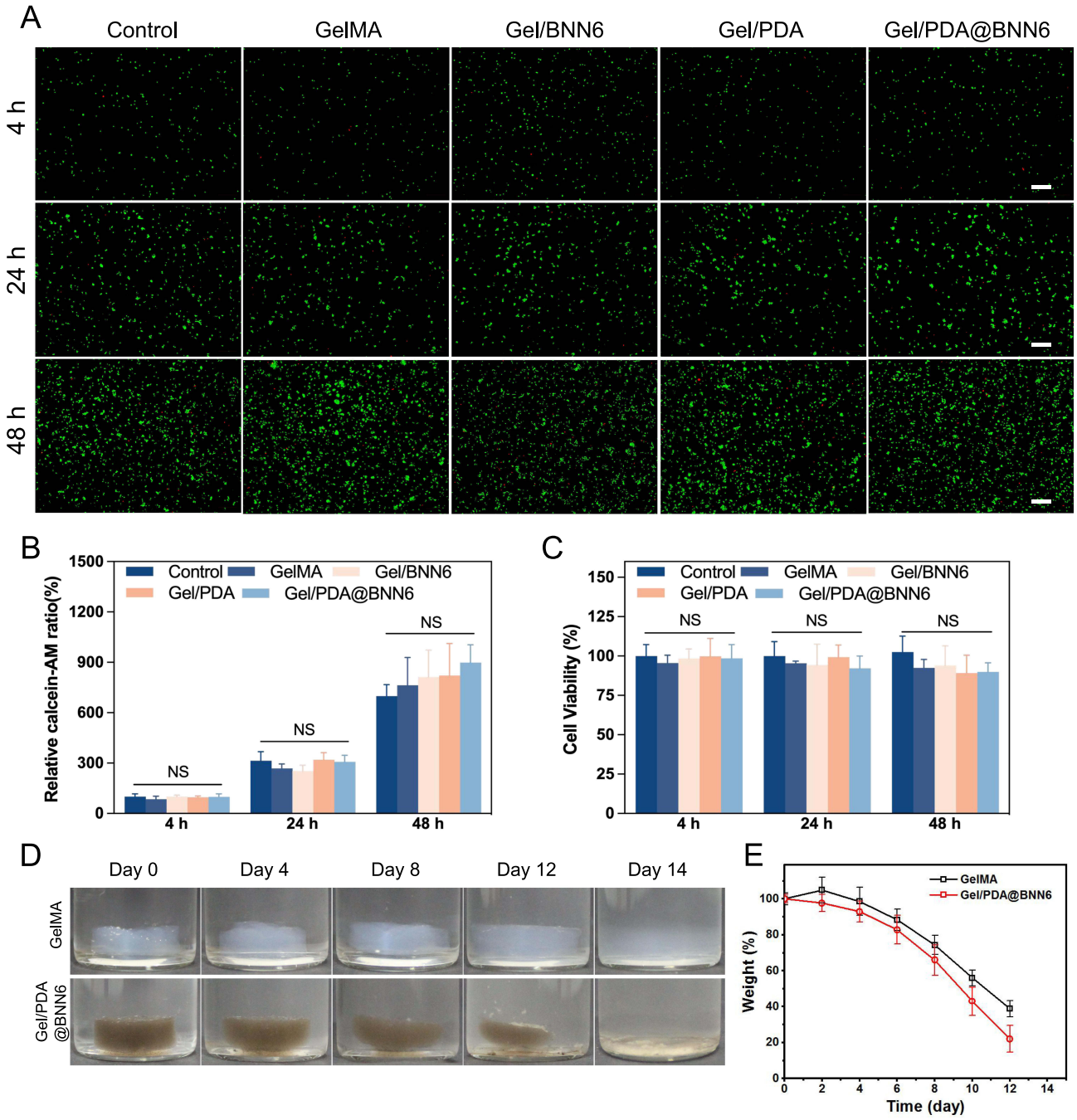

Figure 5 Cytotoxicity assay and degradation characteristics. (**A**) Fluorescent images of HaCaT cells after treatment with different samples (scale bars: 200 μm). (**B**) Relative calcein-AM fluorescence ratio. (**C**) Cell viability by CCK-8 assay (n = 4, NS means not significant). (**D**) Pictures and (**E**) associated statistics of the degradation progress of the GelMA and Gel/PDA@BNN6 (n=3).

indicating that those hypotoxic hydrogels favor HaCaT cell proliferation. Moreover, the cell viability was greater than 90% after 4 and 24 hours of co-culture and 80% after 48 hours for all groups, as shown in Figure 5C. Above all, these results indicate that all hydrogels used in the experiment exhibited excellent biosecurity.

The degradation characteristics of the hydrogels were evaluated in PBS at pH 7.4 and 37 °C. As shown in Figure 5D and E, both hydrogels were wholly degraded after 14 days of mechanical oscillation, indicating that GelMA and Gel/PDA@BNN6 possess auto-degradation properties.

Photothermal Performance and Wound Healing in vivo

A rat model with full-thickness skin infection was constructed to test Gel/PDA@BNN6's therapeutic ability in vivo. With near-infrared irradiation, the skin wound temperature increased to 45.6 °C with Gel/PDA@BNN6 treatment. The temperature of the local tissue of the Gel/PDA treatment increased to 44.0°C (Figure 6A and B). This phenomenon proved that the hydrogels also have a favorable photothermal property in vivo.

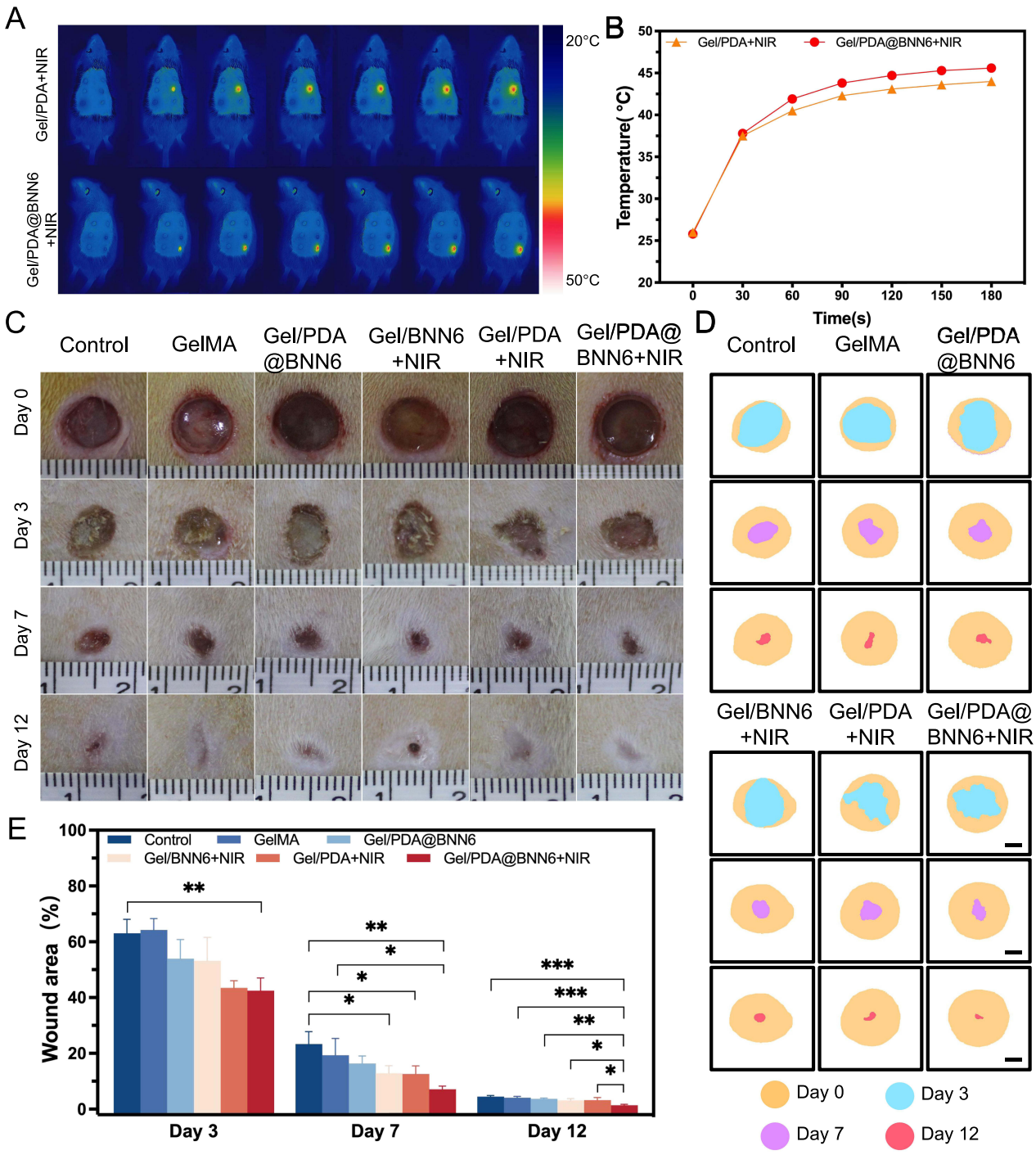

Figure 6 In vivo wound healing experiment: (**A**) The imagery of the wound sites infrared thermally and (**B**) the corresponding temperature increase curve. (**C**) Visual view of the wound healing process. (**D**) Wound site Model drawing after treatment on days 0 through 12 (scale bars: 2 mm). (**E**) The wound area was quantified in all groups (n = 3, *p < 0.05, **p < 0.01 and ***p < 0.001).

Next, we assessed the rate of wound healing by recording changes in wound contraction and mapping the corresponding area schematically (Figure 6C and D). By 3 days after the surgery, it was evident that all groups had developed some level of pus exudation, confirming the successful creation of the infected wound model. However, the Gel/PDA@BNN6 + NIR group displayed the least severe infection reaction, attributed to the superior sterilization ability of the NIR-functionalized hydrogel. Compared with the control, Gel/BNN6 + NIR and Gel/PDA + NIR treatments exhibited higher healing efficiency after 7 days postoperatively. On day 12, the wound area of control, GelMA, Gel/PDA@BNN6, Gel/BNN6 + NIR, Gel/PDA + NIR and Gel/PDA@BNN6 + NIR reduced to 4.52%, 4.07%, 3.7%, 3.19%, 3.26%, and 1.41%, respectively. There were apparent differences in wound healing rates between Gel/PDA@BNN6 + NIR and other groups (Figure 6E). Independent application of either the photothermal reaction or nitric oxide promotes wound contraction to a certain extent. However, the dual-action approach of Gel/PDA@BNN6 achieves better results by utilizing near-infrared light to catalyze the release of nitric oxide and synergize the photothermal effect. These results provided intuitive evidence that NIR-functionalized Gel/PDA@BNN6 was an excellent dressing with anti-infective action and accelerated wound healing.

Histomorphological Analysis

12 days after surgery, we stained wound tissue with H&E and Masson's trichrome to assess wound healing. H&E and Masson's trichrome staining showed regenerated epidermal tissue in all groups (Figure 7A and B). However, compared to the other groups, injuries treated with Gel/PDA@BNN6 + NIR showed complete epidermal and dermal regeneration, more new glands, and increased proliferation of fibroblasts. Most importantly, the structure of the Gel/PDA@BNN6 +

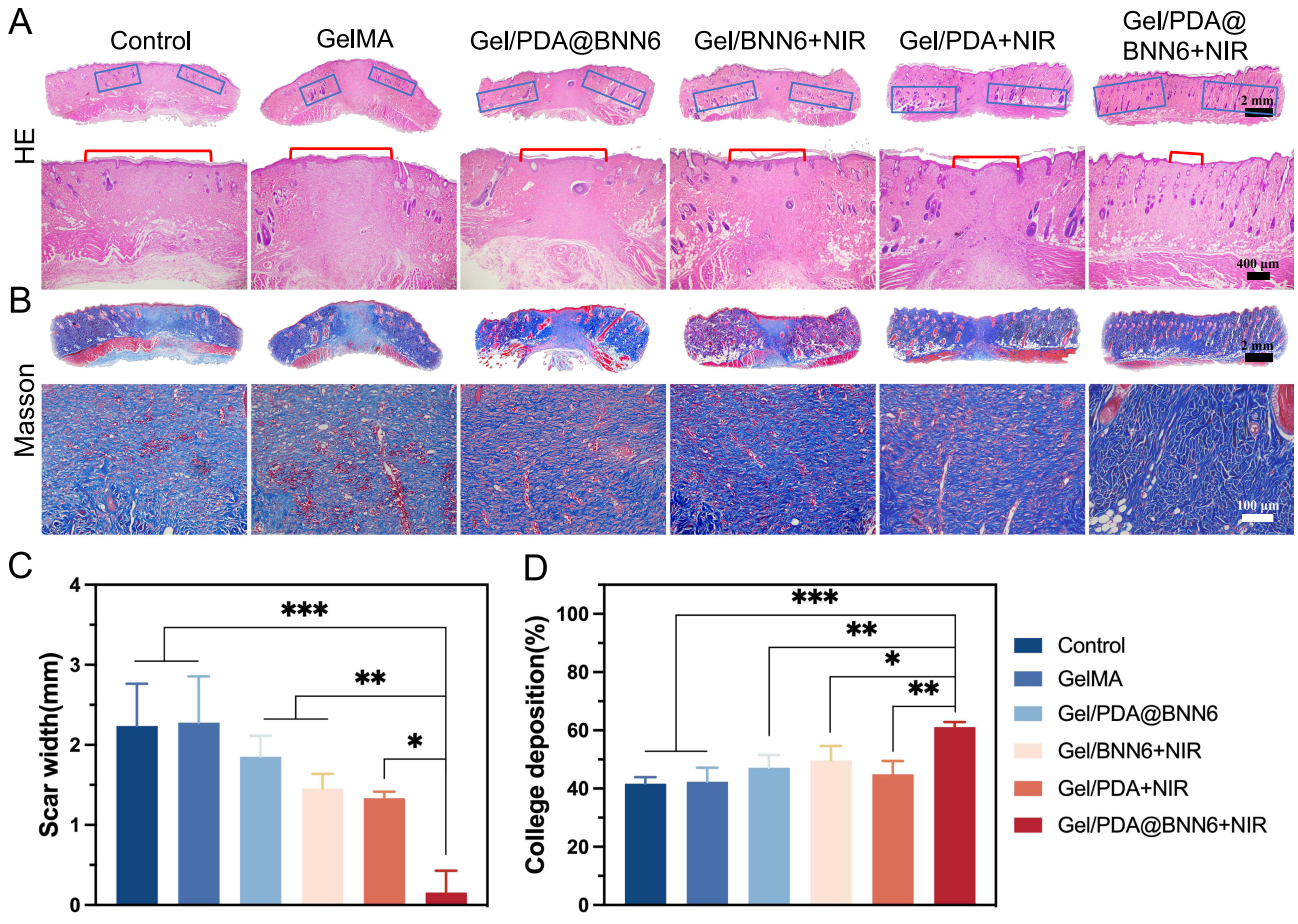

Figure 7 Histological assessment of wounded areas 12 days post-operatively. (**A**) HE staining (The wound area is shown in red fields and newly growing hair follicles are shown in blue squares). (**B**) Masson staining. (**C**) and (**D**) Quantitative analysis of histological stained images: scar width, collagen deposition (n = 3, *P < 0.05, **P < 0.01, and ***P < 0.001).

NIR group of wounds was closest to the surrounding normal tissue. In addition, we statistically analyzed scar width and collagen deposition (Figure 7C and D). We found that the GelMA group had results consistent with the control group, indicating that GelMA had good biocompatibility to be used as a biological dressing. Figure 7C showed that both Gel/PDA@BNN6 + NIR and the Gel/PDA + NIR wounds were smaller, which meant photothermal properties could positively affect wound healing. Meanwhile, the difference between the two groups demonstrated that NO could reduce the size of the damage. The efficacy of wound closure in the Gel/PDA@BNN6 group appeared weak, as it relied solely on the spontaneous release of nitric oxide. Collagen can promote keratinocyte migration and contribute to wound re-epithelialization.[44] From Figure 7D, the collagen proteins of the groups with BNN6 added are increased compared to the other groups due to NO's ability to promote collagen deposition. It is evident that the Gel/PDA@BNN6 + NIR therapy expedited wound healing and boosted collagen deposition, thereby decreasing the possibility of scarring.

Immunohistochemical staining for inflammatory factors (IL-6 and CD163) was performed to analyze wound inflammation following 12 days of therapy. (Figure 8A and B). In the later stages of the inflammatory response, M2 phenotype macrophages marked by CD163 could inhibit the inflammatory response, secrete growth factors, recruit fibroblasts, and accelerate myofibroblast transition, thus promoting wound healing.[5,45] Figure 8D and E illustrated that the control and GelMA groups had a mass of IL-6 secretion and a few scattered CD163, delivering a robust inflammatory response in these groups. A little IL-6 secretion and more CD163 were scattered in the Gel/PDA@BNN6 + NIR group, Gel/PDA + NIR group, and Gel/BNN6 + NIR group, which is due to the bactericidal effect of the photothermal therapy combined with modulated inflammation by NO, resulting in a milder inflammatory response.

The amount of neovascularization is crucial to granulation tissue regeneration and wound repair. Endothelial cell marker CD31 and fibroblast marker α-SMA could evaluate mature vascular structures. As observed in the results of the immunofluorescence staining (Figure 8C), the Gel/PDA@BNN6 + NIR group had the highest levels of CD31, which was 1.25%, followed by the Gel/BNN6 + NIR group (Figure 8F). In line with the trend of CD31,

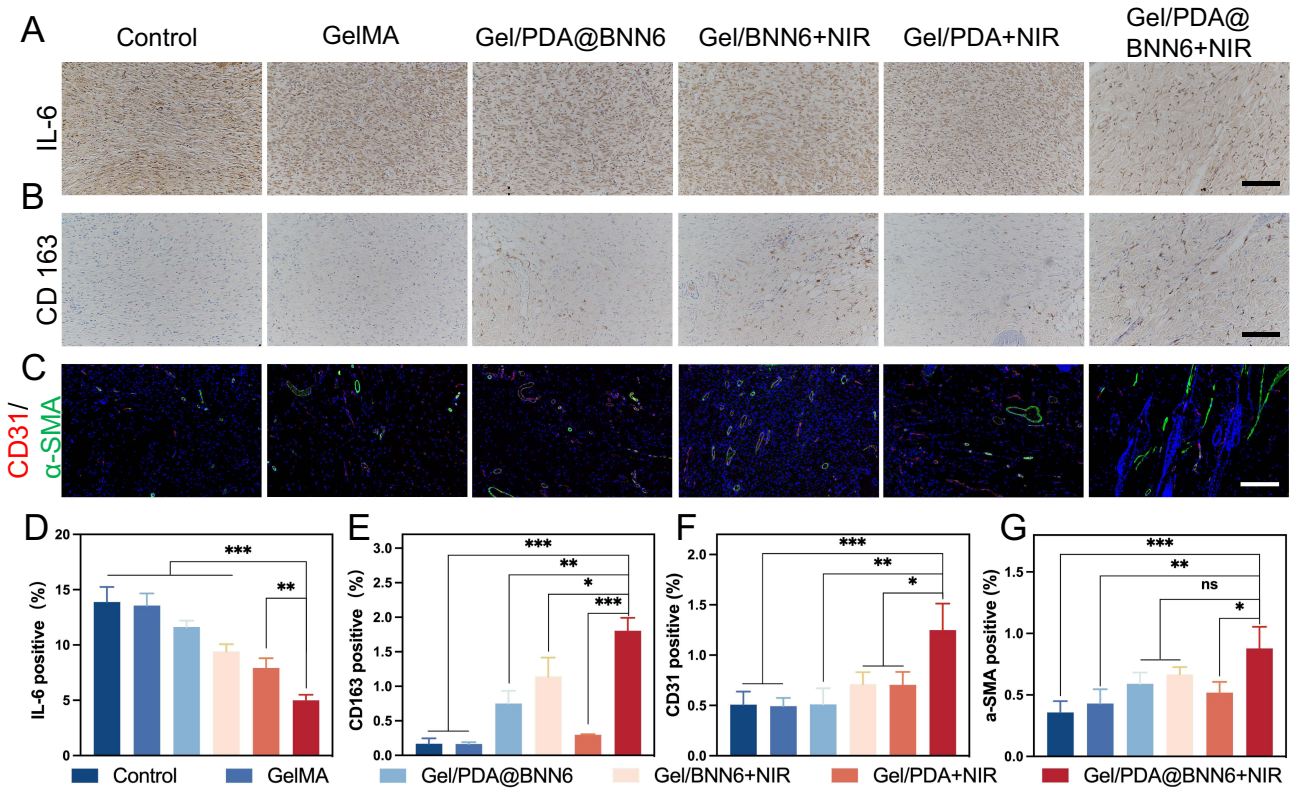

Figure 8 Immunohistochemical staining analysis of wound tissue was performed on day 12 after surgery. (**A**) IL-6 staining and (**D**) corresponding positive rate. (**B**) CD163 staining and (**E**) corresponding positive rate. (**C**) Immunofluorescence staining for inflammatory CD31 (red) and angiogenic a-SMA (green) and (**F** and **G**) corresponding positive rate. (n = 3, ns means not significant, *P < 0.05, **P < 0.01, and ***P < 0.001, scale bars: 200 μm).

the statistical analysis of α-SMA levels revealed that the Gel/PDA@BNN6 + NIR group showed a blood vessel density of 0.88%, indicating a higher number of mature blood vessels (Figure 8G). These results indicate that the Gel/PDA@BNN6 + NIR therapy has significant potential for treating infected wounds.

H&E staining of postoperative rats' hearts, livers, spleens, lungs, and kidneys of postoperative rats showed no abnormalities (Figure S7). Blood biochemical indices for liver and kidney function remained normal (Figure S8). So, the Gel/PDA@BNN6 has good biocompatibility in vivo, making it a promising option for related therapies.

Conclusion

In this paper, we developed a nanoparticle composite hydrogel demonstrating exceptional antibacterial and wound-healing effects. The hydrogel forms by PDA@BNN6 nanoparticles encapsulated in GelMA using the UV polymerization method. The nanocomposite hydrogel dressing demonstrated excellent material stability, mechanical strength, and biocompatibility in vitro. The photothermal properties of PDA NPs achieve controlled NO release, resulting in superior antibacterial efficacy both in vitro and in vivo. In the rat experiment, Gel/PDA@BNN6 combined NIR therapy demonstrated sterilization, anti-inflammatory properties, collagen deposition, angiogenesis acceleration promotion, and speeds wound healing. In brief, this photothermal responsive NO-delivering nanocomposite hydrogel presents an ideal treatment for clinical infectious wounds.

Acknowledgments

This work was funded by the Hubei Provincial Central Guidance Local Science and Technology Development Project (2022BGE264), the Health Commission of Hubei Provincial (WJ2023Q017, WJ2023M130), and the Wuhan Knowledge Innovation Project (2022020801010546, 2023020201020546).

Disclosure

The authors declare no conflict of interest.

References

1. Harris-Tryon TA, Grice EA. Microbiota and maintenance of skin barrier function[J]. *Science*. 2022;376(6596):940–945. doi:10.1126/science.abo0693
2. Chambers ES, Vukmanovic-Stejic M. Skin barrier immunity and ageing[J]. *Immunology*. 2020;160(2):116–125. doi:10.1111/imm.13152
3. M TE, Dorati R, Genta I, et al. Skin wound healing process and new emerging technologies for skin wound care and regeneration[J]. *Pharmaceutics*. 2020;12(8):735. doi:10.3390/pharmaceutics12080735
4. L ZY, Wang C, Q YX, et al. Multifunctional xyloglucan-containing electrospun nanofibrous dressings for accelerating infected wound healing[J]. *Int J Biol Macromol*. 2023;247:125504. doi:10.1016/j.ijbiomac.2023.125504
5. Zhang X, Wu Y, Gong H, et al. A Multifunctional Herb-Derived Glycopeptide Hydrogel for Chronic Wound Healing[J]. *Small*. 2024:2400516. doi:10.1002/smll.202400516
6. Yang Y, Liang Y, Chen J, et al. Mussel-inspired adhesive antioxidant antibacterial hemostatic composite hydrogel wound dressing via photo-polymerization for infected skin wound healing[J]. *Bioact Mater*. 2022;8:341–354. doi:10.1016/j.bioactmat.2021.06.014
7. Zhang S, He T, Zhao F, et al. Development of a Multifunctional Nano-Hydroxyapatite Platform (nHEA) for Advanced Treatment of Severely Infected Full-Thickness Skin Wounds[J]. *Acta Biomater*. 2024. doi:10.1016/j.actbio.2024.05.005
8. Abazari M, Akbari T, Hasani M, et al. Polysaccharide-based hydrogels containing herbal extracts for wound healing applications[J]. *Carbohydr Polym*. 2022;294:119808. doi:10.1016/j.carbpol.2022.119808
9. Wang H, Xu Z, Zhao M, et al. Advances of hydrogel dressings in diabetic wounds[J]. *Biomater Sci*. 2021;9(5):1530–1546. doi:10.1039/D0BM01747G
10. Lan Y, Wang Y, Qi X, et al. A modified hyaluronic acid hydrogel with strong bacterial capture and killing capabilities for drug-resistant bacteria-infected diabetic wound healing[J]. *Int J Biol Macromol*. 2024;279:135301. doi:10.1016/j.ijbiomac.2024.135301
11. Rastin H, T OR, J AG, et al. 3D bioprinting of methylcellulose/gelatin-methacryloyl (MC/GelMA) bioink with high shape integrity[J]. *ACS Appl. Bio Mater*. 2020;3(3):1815–1826. doi:10.1021/acsabm.0c00169
12. Liu S, Zhao Y, Li M, et al. Bioactive wound dressing based on decellularized tendon and GelMA with incorporation of PDA-loaded asiaticoside nanoparticles for scarless wound healing[J]. *Chem Eng J*. 2023;466:143016. doi:10.1016/j.cej.2023.143016
13. Qi X, Shi Y, Zhang C, et al. A Hybrid Hydrogel with Intrinsic Immunomodulatory Functionality for Treating Multidrug-Resistant Pseudomonas aeruginosa Infected Diabetic Foot Ulcers[J]. *ACS Mater Lett*. 2024;6:2533–2547. doi:10.1021/acsmaterialslett.4c00392
14. Liang C, Wang H, Lin Z, et al. Augmented wound healing potential of photosensitive GelMA hydrogel incorporating antimicrobial peptides and MXene nanoparticles[J]. *Front Bioeng Biotechnol*. 2023;11. doi:10.3389/fbioe.2023.1310349
15. Liang Z, Liu W, Wang Z, et al. Near-infrared laser-controlled nitric oxide-releasing gold nanostar/hollow polydopamine Janus nanoparticles for synergistic elimination of methicillin-resistant Staphylococcus aureus and wound healing[J]. *Acta Biomater*. 2022;143:428–444. doi:10.1016/j.actbio.2022.02.029

16. Liu G, Wang L, He Y, et al. Polydopamine nanosheets doped injectable hydrogel with nitric oxide release and photothermal effects for bacterial ablation and wound healing[J]. *Adv. Healthcare Mater*. 2021;10(23):2101476. doi:10.1002/adhm.202101476
17. Zeng B, Mu Z, Shen T, et al. A self-propelled nanovesicle with robust antibacterial and regeneration-promoting capabilities for treating biofilm-induced periodontitis[J]. *Chin. Chem. Lett*. 2024:110350. DOI:10.1016/j.cclet.2024.110350
18. Zhang M, Fan Z, Zhang J, et al. Multifunctional chitosan/alginate hydrogel incorporated with bioactive glass nanocomposites enabling photothermal and nitric oxide release activities for bacteria-infected wound healing[J]. *Int J Biol Macromol*. 2023;232:123445. doi:10.1016/j.ijbiomac.2023.123445
19. Zhu J, Jin Q, Zhao H, et al. Reactive oxygen species scavenging sutures for enhanced wound sealing and repair[J]. *Small Struct*. 2021;2(7):2100002. doi:10.1002/sstr.202100002
20. H SC, P LW, C TL, et al. Enhancing microcirculation on multitriggering manner facilitates angiogenesis and collagen deposition on wound healing by photoreleased NO from hemin-derivatized colloids[J]. *ACS nano*. 2019;13(4):4290–4301. doi:10.1021/acsnano.8b09417
21. C LP, N SA, A BG, et al. Impaired wound healing and angiogenesis in eNOS-deficient mice[J]. *Am J Physiol Heart Circ Physiol*. 1999;277(4):H1600–H1608. doi:10.1152/ajpheart.1999.277.4.H1600
22. Yamasaki K, D EH, McClosky C, et al. Reversal of impaired wound repair in iNOS-deficient mice by topical adenoviral-mediated iNOS gene transfer[J]. *J Clin Invest*. 1998;101(5):967–971. doi:10.1172/JCI2067
23. K WK, Xu X, Wu M, et al. MDM2 induces pro-inflammatory and glycolytic responses in M1 macrophages by integrating iNOS-nitric oxide and HIF-1α pathways in mice[J]. *Nat Commun*. 2024;15(1):8624. doi:10.1038/s41467-024-53006-w
24. Postat J, Olekhnovitch R, Lemaître F, et al. A metabolism-based quorum sensing mechanism contributes to termination of inflammatory responses[J]. *Immunity*. 2018;49(4):654–665.e5. doi:10.1016/j.immuni.2018.07.014
25. Xiang G, Wang B, Zhang W, et al. A Zn-MOF-GOx-based cascade nanoreactor promotes diabetic infected wound healing by NO release and microenvironment regulation[J]. *Acta Biomater*. 2024:245–259. DOI:10.1016/j.actbio.2024.05.015
26. Yao S, Wang Y, Chi J, et al. Porous MOF microneedle array patch with photothermal responsive nitric oxide delivery for wound healing[J]. *Adv. Sci*. 2022;9(3):2103449. doi:10.1002/advs.202103449
27. Gao D, Chen T, Chen S, et al. Targeting hypoxic tumors with hybrid nanobullets for oxygen-independent synergistic photothermal and thermodynamic therapy[J]. *Nano-Micro Lett*. 2021;13:1–21. doi:10.1007/s40820-021-00616-4
28. Lv X, Xu Y, Ruan X, et al. An injectable and biodegradable hydrogel incorporated with photoregulated NO generators to heal MRSA-infected wounds[J]. *Acta Biomater*. 2022;146:107–118. doi:10.1016/j.actbio.2022.05.006
29. Huang S, Liu H, Liao K, et al. Functionalized GO nanovehicles with nitric oxide release and photothermal activity-based hydrogels for bacteria-infected wound healing[J]. *ACS Appl Mater Interfaces*. 2020;12(26):28952–28964. doi:10.1021/acsami.0c04080
30. Zhang P, Xu X, He W, et al. Autocatalytically hydroxyl-producing composite wound dressing for bacteria-infected wound healing[J]. *Nanomed Nanotechnol Biol Med*. 2023;51:102683. doi:10.1016/j.nano.2023.102683
31. N ZW, Wang D, P YQ, et al. Near-infrared light-controllable multifunction mesoporous polydopamine nanocomposites for promoting infected wound healing[J]. *ACS Appl. Mater Interfaces*. 2022;14(2):2534–2550. doi:10.1021/acsami.1c19209
32. Guo F, Chen J, Zhao J, et al. Z-scheme heterojunction g-C3N4@ PDA/BiOBr with biomimetic polydopamine as electron transfer mediators for enhanced visible-light driven degradation of sulfamethoxazole[J]. *Chem Eng J*. 2020;386:124014. doi:10.1016/j.cej.2020.124014
33. Yan S, Liao X, Xiao Q, et al. Photostabilities and anti-tumor effects of curcumin and curcumin-loaded polydopamine nanoparticles[J]. *RSC Adv*. 2024;14(20):13694–13702. doi:10.1039/D4RA01246A
34. Liu L, Wang Q, Liao H, et al. Soluble microneedle patch with photothermal and NO-release properties for painless and precise treatment of ischemic perforator flaps[J]. *J Mat Chem B*. 2021;9(37):7725–7733. doi:10.1039/D1TB00491C
35. Batul R, Bhave M, Mahon PJ, Yu A. Polydopamine nanosphere with in-situ loaded gentamicin and its antimicrobial activity. *Molecules*. 2020;25(9). doi:10.3390/molecules25092090
36. Gao Q, Zhang X, Yin W, et al. Functionalized MoS2 nanovehicle with near-infrared laser-mediated nitric oxide release and photothermal activities for advanced bacteria-infected wound therapy[J]. *Small*. 2018;14(45):1802290. doi:10.1002/smll.201802290
37. Yuan M, Liu K, Jiang T, et al. GelMA/PEGDA microneedles patch loaded with HUVECs-derived exosomes and Tazarotene promote diabetic wound healing[J]. *J Nanobiotechnol*. 2022;20(1):147. doi:10.1186/s12951-022-01354-4
38. Zuo Y, Liu X, Wei D, et al. Photo-cross-linkable methacrylated gelatin and hydroxyapatite hybrid hydrogel for modularly engineering biomimetic osteon. *ACS Appl Mater Interf*. 2015;7:10386–10394. doi:10.1021/acsami.5b01433
39. Kumankuma-Sarpong J, Chang C, Hao J, et al. Entanglement Added to Cross-linked Chains Enables Tough Gelatin-based Hydrogel for Zn Metal Batteries[J]. *Adv Mater*. 2024:2403214. doi:10.1002/adma.202403214
40. Lan L, Ping J, Li H, et al. Skin-Inspired All-Natural Biogel for Bioadhesive Interface[J]. *Adv Mater*. 2024:2401151. doi:10.1002/adma.202401151
41. Mouser VHM, Melchels FPW, Visser J, Dhert WJA, Gawlitta D, Malda J. Yield stress determines bioprintability of hydrogels based on gelatin-methacryloyl and gellan gum for cartilage bioprinting. *Biofabrication*. 2016;8:035003. doi:10.1088/1758-5090/8/3/035003
42. Li Y, Xu T, Tu Z, et al. Bioactive antibacterial silica-based nanocomposites hydrogel scaffolds with high angiogenesis for promoting diabetic wound healing and skin repair[J]. *Theranostics*. 2020;10(11):4929. doi:10.7150/thno.41839
43. Yu S, Li G, Zhao P, et al. NIR-laser-controlled hydrogen-releasing PdH nanohydride for synergistic hydrogen-photothermal antibacterial and wound-healing therapies[J]. *Adv Funct Mater*. 2019;29(50):1905697. doi:10.1002/adfm.201905697
44. Mathew-Steiner SS, Roy S, Sen CK. Collagen in wound healing[J]. *Bioengineering*. 2021;8(5):63. doi:10.3390/bioengineering8050063
45. Xu N, Gao Y, Li Z, et al. Immunoregulatory hydrogel decorated with Tannic acid/Ferric ion accelerates diabetic wound healing via regulating Macrophage polarization[J]. *Chem Eng J*. 2023;466:143173. doi:10.1016/j.cej.2023.143173